Estuarine, Coastal and Shelf Science 211 (2018) 137–151

Contents lists available at ScienceDirect

Estuarine, Coastal and Shelf Science

journal homepage: www.elsevier.com/locate/ecss

Phytoplankton bloom dynamics in turbid, well-mixed estuaries: A model study

Bo Liu [a, *], Huib E. de Swart [a], Victor N. de Jonge [b]

[a] Institute for Marine and Atmospheric Research, Utrecht University, Princetonplein 5, 3584 CC, Utrecht, The Netherlands
[b] Institute of Estuarine and Coastal Studies, University of Hull, Hull, HU6 7RX, United Kingdom

ARTICLE INFO

Article history:
Received 16 March 2017
Received in revised form
21 December 2017
Accepted 11 January 2018
Available online 31 January 2018

Keywords:
Phytoplankton growth
Suspended particulate matter
Subtidal current
Seasonal cycle
The Ems estuary
Exploratory model

ABSTRACT

To gain insight into mechanisms underlying phytoplankton bloom dynamics in turbid, well-mixed estuaries, experiments were conducted with an exploratory model that couples physical and biological processes. The motivation for choosing exploratory models is that they allow investigation of individual processes in isolation, therefore yielding fundamental insight into the mechanisms of the system. The Ems estuary (between the Netherlands and Germany) was selected as the prototype estuary, in which a zone of high turbidity is observed in the middle and upper reach. Results show that the model is capable of capturing the main features of the observed phytoplankton population density (P) patterns, that is, in the lower reach a spring bloom occurs, followed by a secondary bloom in autumn. Results of sensitivity studies reveal that the along-estuary distribution of suspended particulate matter (SPM) is a determining factor for the along-estuary location of blooms and it largely affects the intensity of blooms. The along-estuary advection of nutrients by the subtidal current is important for obtaining blooms with high intensities. In this model, the seasonally varying water temperature has a larger impact on the timing of spring blooms than the seasonally varying incident light intensity. The occurrence of an autumn bloom is due to the fact that during the summer season, the net specific growth rate of phytoplankton decreases. The latter is likely to result from an optimum water temperature (smaller than the maximum water temperature) for phytoplankton growth. Nevertheless, the occurrence and characteristics of autumn blooms are also influenced by seasonal variations in other aspects, for instance, loss of phytoplankton due to grazing.

1. Introduction

Phytoplankton blooms are common features in many estuaries. Their occurrence is the result of a joint action of biological processes and physical processes (see Cloern et al., 2014, and references herein). Aspects that influence phytoplankton gross growth are seasonal variation in incident light (Sverdrup, 1953; Domingues et al., 2017), seasonal variation in water temperature (Eppley, 1972; Butterwick et al., 2005) and nutrient limitation (Tilman et al., 1982; Cira et al., 2016). Local nutrient concentrations in estuaries are often proportional to the magnitude of the river discharge (de Jonge and Essink, 1991; van Beusekom and de Jonge, 1998) and their distribution is influenced by advective and mixing processes. The latter two processes also directly impact the spatial distribution of phytoplankton and thus affect the behaviour of blooms (Lucas et al., 1999; Liu and de Swart, 2015). The loss of phytoplankton is determined by processes such as natural death, viral infection (Brussaard, 2004) and pelagic grazing (Lionard et al., 2005).

Availability of light in water is strongly determined by intensity and spatial distribution of suspended particulate matter (hereafter SPM) (Colijn, 1982). Indeed, May et al. (2003) demonstrated that in their model phytoplankton biomass decreases if SPM concentration becomes high. Arndt et al. (2007) demonstrated that in their coupled hydrodynamic, SPM and biochemical model of the Scheldt estuary high values of phytoplankton population density (hereafter denoted as P) are restricted to the upper freshwater reach where SPM concentrations are relatively low. Other model studies (e.g. Camacho et al., 2015; Lopes et al., 2015) have also indicated the importance of light-limited growth at high SPM concentrations.

The above mentioned factors and processes that influence phytoplankton blooms features usually act in concert. In particular,

* Corresponding author.
E-mail address: bo.liu@mpimet.mpg.de (B. Liu).

https://doi.org/10.1016/j.ecss.2018.01.010
0272-7714/

changes in subtidal currents (i.e., tidally-averaged currents), which could result from changes in river discharge, tidal currents, etc., lead to modifications of nutrient, SPM and phytoplankton transport. Furthermore, the effect of the seasonally varying incident light on triggering spring blooms is not distinguishable from that of the seasonally varying water temperature because the latter factor is dependent on the former. These mutual dependencies cause difficulty in understanding field data and in interpreting results of simulation models (in which many processes/factors and their interactions are included).

The overall objective of this study is to gain further insight into mechanisms governing phytoplankton bloom dynamics in turbid, well-mixed estuaries. The specific aims are to quantify and understand the effect of two combinations of dependent control factors on phytoplankton bloom dynamics: 1) SPM distribution and subtidal current, 2) seasonally varying incident light intensity and water temperature. The specific characteristics that will be examined are the intensity, along-estuary location and timing of blooms.

To fulfil these aims, an adapted version of the exploratory model developed by Liu and de Swart (2015) will be considered. As is reviewed by Murray (2003), exploratory models are designed to search for the clearest, simplest answer to the question: which processes or feedbacks produce a specific poorly understood phenomenon. For this purpose, these models include as few processes as possible, while capturing the gross features of that phenomenon. As the model is highly simplified, its behaviour can be understood and processes can be identified which are responsible for the occurrence of the phenomenon. Thus, in exploratory models, the focus is not on obtaining an accurate match with observations, but on simplifying the formalism to find the essential mechanisms. This study employs an exploratory model, with which the combined impacts of SPM distribution, subtidal currents and of seasonally varying incident light intensity and water temperature can be investigated in isolation. In this way, it yields fundamental insight into phytoplankton bloom dynamics in turbid, well-mixed estuaries. Moreover, this model is fast and flexible and is therefore suitable for sensitivity studies (Murray and Thieler, 2004). The highly turbid Ems estuary, located at the German - Dutch border is chosen as the prototype estuary in this study. This estuary is selected as an example because sufficient data on SPM (Talke et al., 2009b; de Jonge et al., 2014), and on nutrients and *P* distributions (Brinkman et al., 2014) are available to check the performance of the model.

The biological module that describes phytoplankton and nutrient dynamics, the hydrodynamical and SPM module, as well as the turbulence closure module are introduced in Section 2. In Section 3, it is first demonstrated that the model is capable of capturing main characteristics of the blooms observed by Brinkman et al. (2014). Here, the comparison between results of the exploratory model and field data focuses on the key features rather than quantitative accuracy. Next, results of sensitivity experiments are presented. In Section 4, the effects of key processes on bloom dynamics are quantified, the effect of the two combinations of control factors are further analysed and consequences of several assumptions of the model are discussed. Conclusions are given in Section 5. In Electronic Supplement 1, results of additional sensitivity studies (which concern boundary and initial conditions, as well as other biological parameters) are presented and analysed.

2. Material and methods

2.1. Model

The exploratory model used in this study is an extended version of that of Liu and de Swart (2015). Phytoplankton and nutrient dynamics are described in a biological module, which is coupled to a hydrodynamic module that contains equations for subtidal currents and to a module that computes tidally-averaged suspended particulate matter (SPM) concentration. The values of input parameters referred to in this section are brought together in Table 1 (see Section 2.3).

2.1.1. Domain

The estuarine geometry considered in this study is displayed in Fig. 1. It represents a channel with length L and it has a rectangular cross section with a constant water depth H. The width b exponentially decreases from a value b_0 at the estuary mouth towards the river head. A Cartesian coordinate system is used, with the x-axis pointing from the estuary mouth ($x = 0$) to the river head ($x = L$) and the z-axis from the water surface ($z = 0$) downward to the bottom ($z = H$). Thus, b is modelled as

$$b(x) = b_0 \exp\left(-\frac{x}{L_b}\right), \tag{1}$$

with L_b the width convergence length scale of the estuary.

2.1.2. Biological module

The biological module follows that of Huisman et al. (2006). The biological processes accounted for are the gross growth and loss of phytoplankton, the uptake of nutrient by phytoplankton and the recycling of nutrients from dead phytoplankton back into the water column. The equations governing phytoplankton and nutrient dynamics are

$$\frac{\partial P}{\partial t} = \mu P - mP - v\frac{\partial P}{\partial z} - u\frac{\partial P}{\partial x} - w\frac{\partial P}{\partial z} + \frac{1}{b}\frac{\partial}{\partial x}\left(b\kappa_h\frac{\partial P}{\partial x}\right) + \frac{\partial}{\partial z}\left(\kappa_v\frac{\partial P}{\partial z}\right), \tag{2}$$

$$\frac{\partial N}{\partial t} = -\alpha\mu P + \varepsilon\alpha mP - u\frac{\partial N}{\partial x} - w\frac{\partial N}{\partial z} + \frac{1}{b}\frac{\partial}{\partial x}\left(b\kappa_h\frac{\partial N}{\partial x}\right) + \frac{\partial}{\partial z}\left(\kappa_v\frac{\partial N}{\partial z}\right). \tag{3}$$

In the above equations, P (a function of x, z, and t) denotes the width-averaged phytoplankton population density (cells m^{-3}) and N (depending on x, z, and t) is the width-averaged nutrient concentration (mmol m^{-3}). Furthermore, μ is the specific growth rate of phytoplankton, m is the loss rate, v is the sinking velocity, α is the nutrient amount in each cell and ε is the proportion of dead phytoplankton that is subsequently recycled. Moreover, u and w are the along-estuary and the vertical velocity, respectively. Finally, κ_h and κ_v are the along-estuary and the vertical turbulent diffusivity, respectively. The terms on the right-hand side of Eq. (2) represent specific growth, loss, sinking, along-estuary advection, vertical advection, along-estuary mixing and vertical mixing of phytoplankton, respectively. Those on the right-hand side of Eq. (3) result from uptake of nutrient by phytoplankton, recycling of nutrient from dead phytoplankton, advective and mixing processes, respectively.

The specific growth rate μ depends on water temperature T, light intensity I and nutrient concentration N:

$$\mu = \mu_T f(N, I). \tag{4}$$

Here, μ_T describes the dependence of growth rate on temperature and $f(N, I)$ $(0 \le f \le 1)$ accounts for the tempering of the growth rate in the case of nutrient or light limitation. The parameterisation of μ_T is an generalisation of that of Luo et al. (2012) and it reads

Table 1
Values of model parameters for the default experiment. The numbers behind the symbols indicate the sources, which are listed below.

Symbol	Interpretation	Unit	Value
H (1)	water depth	m	7
L (1)	estuary length	km	100
b_0 (1)	width at the estuary mouth $x = 0$	m	8000
L_b (2)	width convergence length scale	km	30
m (3)	loss rate of phytoplankton	day^{-1}	0.1
v (4)	sinking velocity of phytoplankton	m day^{-1}	1.0
α (5)	nutrient amount in each phytoplankton cell	mmol $cell^{-1}$	$1{\cdot}10^{-9}$
ε (5)	nutrient recycling coefficient	dimensionless	0.5
H_N (6)	half-saturation constant of nutrient-limited growth	mmol m^{-3}	0.25
H_I (6)	half-saturation constant of light-limited growth	μmol photons m^{-2} s^{-1}	20
k_p (5)	light absorption coefficient of phytoplankton	m^{-1} (cell m^{-3})$^{-1}$	$6{\cdot}10^{-10}$
k_c (7)	light extinction coefficient by SPM	m^{-1} (kg m^{-3})$^{-1}$	45
k (7)	light extinction coefficient due to other components	m^{-1}	0.4
I_{max} (8)	maximum incident light intensity	μmol photons m^{-2} s^{-1}	400
I_{min} (8)	minimum incident light intensity	μmol photons m^{-2} s^{-1}	10
T_{opt} (9)	optimum water temperature for growth	°C	15
b_T	input parameter for the temperature-dependent growth rate	dimensionless	1.5
μ_{opt} (9)	maximum growth rate attained at T_{opt}	day^{-1}	2.5
μ_0 (9)	growth rate attained at 0°C	day^{-1}	0.8
T_{max} (6)	maximum water temperature	°C	22
T_{min} (6)	minimum water temperature	°C	0
t_δ (6)	time lag with respect to light	day	40
$N\|_{x=L}$ (10)	nutrient concentration at the river head	mmol m^{-3}	3.2
$\overline{P}_0$	initial depth-averaged population density	cells m^{-3}	$5{\cdot}10^{7}$
A_v (11)	vertical eddy viscosity	m^2 s^{-1}	$2.0{\cdot}10^{-3}$
κ_v	vertical turbulent diffusivity	m^2 s^{-1}	$1.5{\cdot}10^{-3}$
κ_h (1)	along-estuary turbulent diffusivity	m^2 s^{-1}	100
Q (1)	river discharge	m^3 s^{-1}	−20
x_c (1)	the position where s is $0.5s_0$	km	43.1
x_δ (1)	the length scale over which s varies	km	14.2
β (1)	coefficient of isohaline contraction	kg m^{-3} psu^{-1}	0.83
s_0 (1)	seawater salinity	psu	30
θ (11)	correction coefficient for baroclinic flow	dimensionless	1.4
ρ_s (12)	density of SPM	kg m^{-3}	$1.5{\cdot}10^{3}$
w_s (11)	settling velocity of SPM	m s^{-1}	$0.8{\cdot}10^{-3}$
c_* (11)	domain averaged SPM	kg m^{-3}	1.0

Sources are (1) Talke et al. (2009a), (2) de Jonge et al. (2014), (3) Arndt et al. (2007), (4) Sarthou et al. (2005), (5) Huisman et al. (2006), (6) derived from data of Brinkman et al. (2014), (7) Colijn (1982), (8) derived from meteorological data on The Royal Netherlands Meteorological Institute Climate Explorer (website: https://climexp.knmi.nl/), (9) derived from data of Colijn (1983), (10) van Beusekom and de Jonge (1998). (11) input parameters, (12) de Jonge et al. (2012).

$$\mu_T = \mu_{opt} \exp\left(- a_T \left| \frac{T - T_{opt}}{\widehat{T}} \right|^{b_T} \right). \tag{5}$$

In this expression, T (in°C) is the water temperature, μ_{opt} is the maximum specific growth rate (when neither nutrient nor light limits the growth, i.e., $f(N,I) = 1$), attained at the optimum water temperature T_{opt}, and $\widehat{T} = 1$°C is a reference temperature. Parameter $a_T = -\left(\frac{\widehat{T}}{T_{opt}}\right)^{b_T} \ln\left(\frac{\mu_0}{\mu_{opt}}\right)$ is chosen such that $\mu_T|_{T=0°C} = \mu_0$, where the latter is input to the model. Shapes of μ_T for different values of parameter b_T are plotted in Fig. 2a. Here, the value of b_T is not smaller than one, such that the derivative of μ_T with respect to T is continuous for all T.

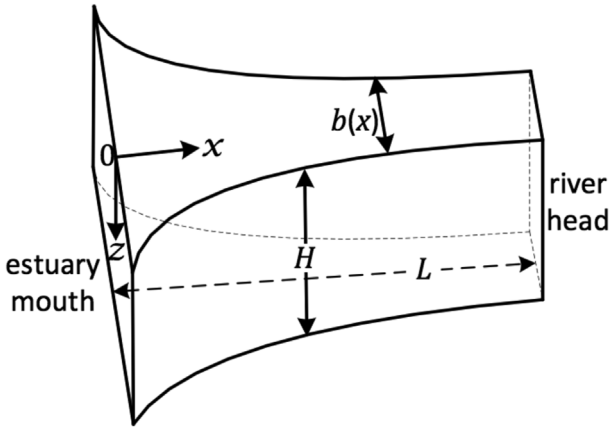

Fig. 1. The configuration of the estuary in the exploratory model. Here, L is the length of the estuary, H is the total water depth, $b(x)$ is the width that exponentially decreases towards the river head and O is the origin of the Cartesian coordinate system.

The parameterisation of the limitation function $f(N,I)$ in this study is proposed by Huisman et al. (2006), and it follows the Monod equation and obeys Von Liebig's 'law of the minimum':

$$f(N,I) = \min\left(\frac{N}{H_N + N}, \frac{I}{H_I + I}\right). \tag{6}$$

Parameters H_N and H_I are the half-saturation constant for nutrient-limited and light-limited growth, respectively, and min denotes the minimum function. Based on the above equation, a limitation index is defined as $\left(\frac{N}{H_N+N} - \frac{I}{H_I+I}\right)$. If the limitation index is negative, phytoplankton growth is nutrient-limited, whilst if the limitation index has positive values, the growth is light-limited. In Fig. 2b, the contour plot of $f(N,I)$ is shown, in which the areas of nutrient- and light-limited growth are indicated.

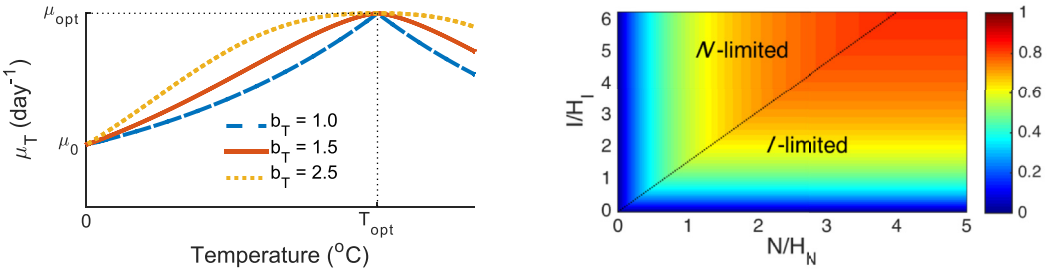

Fig. 2. (a) The shapes of μ_T (Eq. (5)), i.e., the temperature-dependent part of the growth rate versus temperature for different values of b_T. (b) Contour plot of the limitation function $f(N,I)$ (calculated by Eq. (6)). The horizontal axis shows the nutrient concentration N scaled by the half-saturation constant H_N for nutrient-limited growth. The vertical axis shows the light intensity I divided by the half-saturation constant H_I for light-limited growth. The areas of nutrient (N)-limited and light (I)-limited growth are indicated, respectively.

The light is supplied at the water surface. Due to self shading effect of phytoplankton, attenuation by SPM and other substances (for instance, coloured dissolved organic matter), the light intensity in water decreases exponentially with depth according to Lambert-Beer's law:

$$I = I_{in}\exp\left[-k_p\int_0^z P(t,x,z')\mathrm{d}z' - k_c\int_0^z C(x,z')\mathrm{d}z' - k\,z\right]. \tag{7}$$

In this expression, z' is a dummy variable. Parameter I_{in} is the incident light intensity, k_p is the light absorption coefficient of phytoplankton, k_c is the light extinction coefficient by SPM and k is the light extinction coefficient due to the other substances. The tidally-averaged SPM concentration C (in kg m^{-3}) is defined in Section 2.1.3. The incident light intensity I_{in} varies over the seasons and it is modelled as

$$I_{in} = \frac{(I_{max}+I_{min})}{2} - \frac{(I_{max}-I_{min})}{2}\cos\left(2\,\pi\,\frac{t}{T_y}\right). \tag{8}$$

Here, I_{max} and I_{min} are the maximum and minimum incident light intensity, respectively. Furthermore, time t starts at December 21 and T_y represents one year.

The water temperature T also shows seasonal variability. It is modelled as

$$T = \frac{(T_{max}+T_{min})}{2} - \frac{(T_{max}-T_{min})}{2}\cos\left[2\,\pi\,\frac{(t-t_\delta)}{T_y}\right], \tag{9}$$

in which T_{max} and T_{min} are the maximum and minimum water temperature, respectively. Parameter t_δ is the time lag with respect to the incident light intensity and it originates from high heat capacity of water.

The boundary conditions read

$$\left(vP - \kappa_v\frac{\partial P}{\partial z}\right)|_{z=0 \text{ and } z=H} = 0, \quad \left(\kappa_v\frac{\partial N}{\partial z}\right)|_{z=0 \text{ and } z=H} = 0. \tag{10}$$

$$\kappa_h\frac{\partial P}{\partial x}|_{x=0} = 0, \quad \kappa_h\frac{\partial N}{\partial x}|_{x=0} = 0. \tag{11}$$

$$\left(uP - \kappa_h\frac{\partial P}{\partial x}\right)|_{x=L} = 0, \quad N|_{x=L} = N_L. \tag{12}$$

Thus, at the surface and the bottom, zero-flux conditions are applied to P and N (Eq. (10)). At the estuary mouth, diffusive transport of P and N vanishes, whereas along-estuary advection of P and N is allowed (Eq. (11)). At the river head, zero-flux conditions are applied to P (that is, no import of freshwater phytoplankton), since this study focuses on internal growth of phytoplankton in the estuary. Furthermore, a fixed nutrient concentration N_L is imposed at the river head (Eq. (12)).

In the initial state, a depth-averaged population density $\overline{P}_0$ is imposed, i.e., $\overline{P}_0 = (1/H)\int_0^H P_0(z)\,\mathrm{d}z$, which is constant along the estuary. The initial vertical distribution $P_0(z)$ obeys $(vP_0 - \kappa_v\partial P_0/\partial z) = 0$. Furthermore, the initial nutrient concentration N_0 is longitudinally uniform and $N_0 = N_L$ such that the distribution of N_0 obeys the boundary conditions (see Eqs. (10)–(12)) of N.

2.1.3. Hydrodynamic, SPM and turbulent closure module

The estuarine subtidal current and suspended particulate matter (SPM) concentration are modelled as in Talke et al. (2009a, b). Salinity is assumed vertically well mixed, and the tidally-averaged eddy viscosity A_v and diffusivity κ_v are vertically constant. Furthermore, the longitudinal turbulent diffusivity κ_h is spatially constant.

The width-averaged along-estuary velocity $u(x,z)$ (see Eq. S1 in the Electronic Supplement 2) consists of three components. The first is driven by the along-estuary salinity gradient. Here, the depth-averaged salinity $s(x)$ (see Eq. S(5)) is prescribed by using an analytical function that is proposed by Warner et al. (2005). The second component is forced by the along-estuary variation of bottom SPM concentration and the third component is the river flow driven by freshwater discharge. The width-averaged vertical subtidal velocity $w(x,z)$ follows from conservation of water mass (Eq. S(6)).

The vertical distribution (see Eq. S(7)) of the tidally-averaged, width-averaged SPM follows an exponential profile, which results from the assumption that the settling of SPM is balanced by the upward flux of SPM by vertical turbulent mixing. The along-estuary distribution of SPM is calculated by imposing morphodynamic equilibrium (Eq. S(8)), that is, the erosion balances deposition at the bed and hence there is no transport of sediment through any cross-section.

2.2. Model implementation and verification

For a given set of parameter values, the flow due to along-estuary salinity gradient and river flow (see Eq. S1) are calculated algebraically. The calculation of the flow component induced by along-estuary SPM gradient is detailed in Electronic Supplement 2.

The two nonlinear differential equations in the biological module are solved numerically. Central finite difference schemes

are employed for spatial discretisation on a rectangular uniform grid system and a fourth-order Runge-Kutta scheme is used to discretise the time derivatives (Press et al., 1992). This numerical scheme was also used by Liu and de Swart (2015) and it has been verified against data from published studies, such as Huisman et al. (2006), yielding identical results.

2.3. Experimental set-up

2.3.1. Default experiment

At first, an experiment was carried out to verify the capability of the model to simulate the observed phytoplankton blooms in the Ems estuary in year 2013, as reported by Brinkman et al. (2014). This simulation is referred to as the "default experiment". Fig. 3 displays the map of the Ems estuary that extends from the seaward boundary near the island Borkum to the weir at Herbrum, Germany. According to Brinkman et al. (2014), during blooms in 2013, phytoplankton observed in the Ems estuary are dominated by diatoms. Furthermore, the limiting nutrient is phosphorus because field data of the above-cited study showed that in the spring of year 2013, the concentrations of phosphorus in the Ems estuary decreased faster than those of either silicon or nitrogen. The grid has 401×21 grid nodes in the along-estuary and vertical direction, respectively. The time step is $2 \cdot 10^{-4}$day.

The values of model parameters for the default experiment are listed in Table 1, which were adopted from studies listed below the table. The water depth H is an estimate for the domain-averaged estuarine channel depth. The loss rate m is the annual-averaged value of that used by Arndt et al. (2007). The initial depth-averaged population density is a factor of $10^{-3} - 10^{-1}$ of typical P values during blooms (Muylaert and Sabbe, 1999). The maximum and minimum incident light intensity I_{max} and I_{min} are derived as follows. Data of the global radiation (GR) are available from the Royal Netherlands Meteorological Institute (KNMI). The photosynthetically active radiation is usually taken as 45% of GR, and a factor 2.515 is needed to convert W m^{-2} to μmol photons m^{-2}s^{-1} (Brinkman et al., 2014). The formula converting GR data to I_{in} (the intensity of incident light in this study) reads

$$I_{in}\left(\mu\text{mol photons m}^{-2}\text{s}^{-1}\right) = 2.515\,(0.45\,GR)\left(\text{W m}^{-2}\right) \tag{13}$$

The maximum and minimum water temperature are derived from the field data at the estuary mouth given by Brinkman et al. (2014). The time lag t_δ is set to 40 days, such that maximum temperature is reached at the beginning of August in 2013, in accordance with the data.

The light extinction coefficient k_c and k are obtained as follows. The light attenuation in the water column is primarily caused by suspended sediment rather than by phytoplankton (de Jonge, 1983). Thus, Eq. (7) can be approximated by

$$I = I_{in} \exp\left[- k_c \int_0^z C(x,z')\mathrm{d}z' - kz \right]. \tag{14}$$

Using field data, Colijn (1982) developed an empirical relation between the SPM concentration and the light condition in the Ems estuary:

$$I = I_{in} \exp\left[- \left(K_1\, C(x,z)|_{z=1\ \mathrm{m}} - K_2\right) z\right], \tag{15}$$

where $C(x,z)|_{z=1\mathrm{m}}$ is SPM concentration at 1 m below the water surface, $K_1 = 40\ \text{m}^{-1}(\text{kg m}^{-3})^{-1}$ and $K_2 = 0.4\ \text{m}^{-1}$. Comparing the above two equations, it follows that $k = 0.4\ \text{m}^{-1}$. The value of k_c is obtained by fitting Eq. (14) to Eq. (15).

The values of the optimum water temperature T_{opt} for phytoplankton growth, the maximum specific growth rate μ_{opt} attained at T_{opt}, the maximum specific growth rate μ_0 attained at 0 °C are obtained from the lab experiments of Colijn (1983). In the latter study, a field sample was analysed, which contains multiple phytoplankton species.

The modelled SPM distribution was compared with that observed in the year 2005. These data were presented by Talke et al. (2009b) and by de Jonge et al. (2014). The former study reported the SPM concentrations of an longitudinal section in the middle and upper reach of the Ems estuary and the latter study showed the along-estuary profile of the mean annual near-surface SPM concentrations. These data were chosen because they cover the entire estuary, i.e., $0 \le x \le 100$ km. Moreover, the data from de Jonge et al. (2014) and van Maren et al. (2015) suggest that during 2006–2012, changes in SPM in the lower reach are small (< 10%).

The ratio of the vertical turbulent diffusivity to eddy viscosity was set to $\kappa_v/A_v = 0.75$. This is done because SPM causes damping

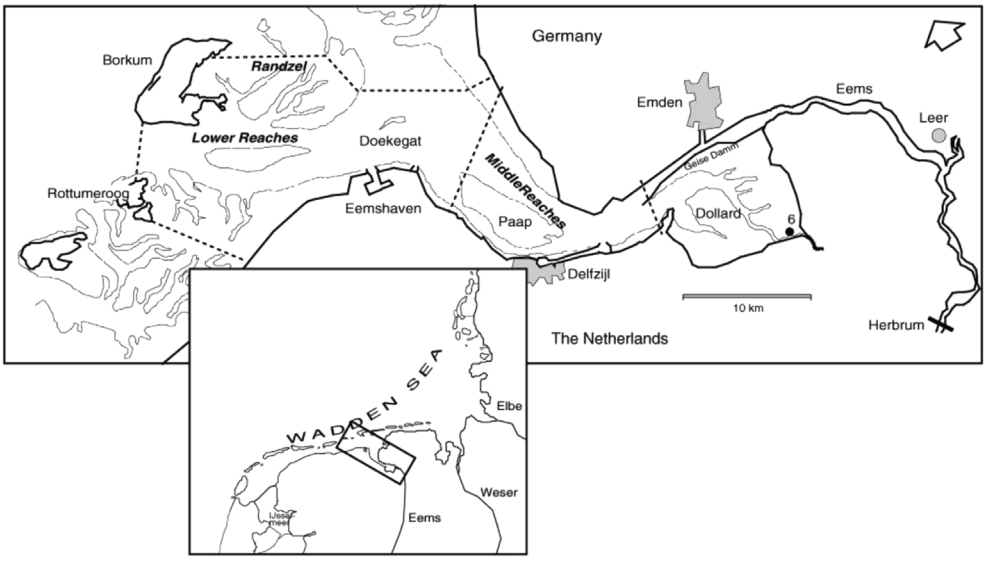

Fig. 3. The map of the Ems estuary from Borkum island to the tidal weir in Herbrum (Germany), reproduced from de Jonge (2000).

of turbulence, which leads to a stronger reduction in κ_v than that in A_v (Munk and Anderson, 1948). The values of A_v and the settling velocity w_s of SPM, together with those of the input parameters θ and c_* (domain-averaged SPM concentration), were chosen to obtain close agreement between modelled and observed SPM concentrations.

To achieve the research aims, further sensitivity experiments were conducted. The set-up of these experiments is summarised in Table 2.

2.3.2. Research aim 1

To distinguish the effects of SPM distribution and subtidal currents on the characteristics of phytoplankton blooms, SPM and subtidal currents were eliminated from the biological module, respectively. Specifically, an experiment was conducted, in which the light attenuation ($-k_c \int_0^z C(x,z')\mathrm{d}z'$, i.e. the second term in Eq. (7)) by SPM was switched off. In another experiment, the advection terms $-u\frac{\partial P}{\partial x}$, $-w\frac{\partial P}{\partial z}$, $-u\frac{\partial N}{\partial x}$ and $-w\frac{\partial N}{\partial z}$ were switched off.

2.3.3. Research aim 2

To separate the impact of seasonally varying incident light intensity I_{in} and water temperature T on bloom characteristics, the seasonal variability of I_{in} and T were switched off, respectively. Specifically, an experiment was carried out with a constant incident light intensity $I_{in,\mathrm{const}} = (I_{max} + I_{min})/2 = 205$ μmol photons m^{-2} s^{-1}. Next, an experiment was conducted with a constant water temperature $T_{\mathrm{const}} = (T_{max} + T_{min})/2 = 11$ °C.

In addition to the above experiments, sensitivity experiments were conducted, in which boundary and initial conditions in the biological module and other biological parameters were varied. These results are presented and discussed in Electronic Supplement 1.

3. Results

The model output of the default experiment is presented in Section 3.1. This is followed, in Section 3.2, by showing results of the sensitivity experiments that are listed in Table 2. For all experiments, after one year of simulation time, phytoplankton population density P and nutrient concentration N reach periodic states with a period of one year. Furthermore, both modelled P and N are vertically almost uniform. Specifically, P values only slightly increase ($<5\%$) towards the bottom. Hence, results shown in this section concern only the depth-averaged phytoplankton population density for one cycle (from January 1st to December 31st) of the periodic states.

3.1. Default experiment

Fig. 4a displays the spatial distribution of the along-estuary subtidal velocity u. Near the estuary mouth ($x<20$ km), u has small values ($<2\cdot10^{-3}$ m s^{-1}). In the area between 20 km and 60 km from the estuary mouth, u is predominantly driven by along-estuary density gradient, resulting in seaward flow close to the water surface and ladward flow near the bottom. Close to the river head ($x>60$ km), river flow is dominant. The along-estuary distributions of the calculated and observed near-surface (1 m below the water surface) SPM concentration are shown in Fig. 4b. Clearly, the overall characteristics of the observed near-surface SPM, that is low values in the area $0 \le x < 40$ km and high values (up to ~ 1 kg m^{-3}) for $x>40$ km, are captured by the modelled near-surface SPM. When viewed in the vertical direction, the calculated SPM increases towards the estuary bed ($z = 7$ m). The maximum SPM concentration at $z = 7$ m is 19 kg m^{-3} and occurs at a distance of about 60 km from the estuary mouth. These gross characteristics of SPM distribution are comparable to those reported by Talke et al. (2009b).

The spatiotemporal behaviour of the depth-averaged phytoplankton population density $\overline{P} = \frac{1}{H}\int_0^H P\,\mathrm{d}z$ during one year is shown in Fig. 4c. From January to March, $\overline{P}$ is constantly low ($<10^7$ cells m^{-3}) in the entire estuary. In April, a spring bloom develops in the lower reach ($0 \le x < 40$ km). In early May, the maximum $\overline{P}$ reaches $48\cdot10^7$ cells m^{-3}. Next, in September–November, a secondary bloom occurs in the vicinity of $x = 30$ km, when $\overline{P}$ attains a value of $16\cdot10^7$ cells m^{-3}. Thus, the exploratory model is able to capture the gross features of the observed phytoplankton bloom behaviour (see Fig. 4d) in the Ems estuary being a spring bloom in the lower reach, followed by a weaker secondary bloom in autumn that occurs somewhat further into the estuary. To directly compare the modelled population density to the observed chlorophyll a concentration, $\overline{P}$ should be multiplied by the cellular carbon content and by the chlorophyll to carbon ratio. Using a cellular carbon content $= 4.6\cdot10^{-6}$ mg cell^{-1} (Godhe et al., 2008) and a chlorophyll:carbon ratio $= 0.02$ mgChla $(\mathrm{mgC})^{-1}$ (de Jonge, 1980; Arndt et al., 2007), the maximum $\overline{P} = 48\cdot10^7$ cells m^{-3} is corresponding to 44 mgChla m^{-3}. Thus, the modelled maximum population density is reasonable.

To examine detailed development of blooms, the location (the gray dashed line in Fig. 4c) of the time-dependent along-estuary maximum depth-averaged population density $\overline{P}_{max}$ is shown. Clearly, $\overline{P}_{max}$ first occurs at the estuary mouth, while later its location gradually shifts landwards. Hereafter, the intensity (denoted as $\overline{P}_{\mathrm{bloom}}$) of a bloom is quantified by the local maxima of $\overline{P}_{max}$ and the timing of a bloom is quantified by the time at which $\overline{P}_{max}$ reaches a local maximum value.

3.2. Sensitivity experiments

The comparison of P patterns between the default experiment and each sensitivity experiment (listed in Table 2) are made via the values of $\overline{P}_{max}$ and the along-estuary locations χ of $\overline{P}_{max}$. Here, χ is the longitudinal distance from the estuary mouth to the site of $\overline{P}_{max}$. These results are shown in Fig. 6a and b. The quantities (including $\overline{P}_{max}$ and χ) that are frequently used to present and discuss model results are summarised in Table 3.

3.2.1. Light attenuation by SPM and advection by subtidal current

When the light attenuation ($-k_c \int_0^z C(x,z')\mathrm{d}z'$) by SPM is discarded, values of $\overline{P}_{max}$ are about one order of magnitude larger than

Table 2
Description of experiments.

Default experiment
Aim 1 – effect of SPM distribution and subtidal current on bloom characteristics.
• As the default experiment, but for the attenuation ($-k_c \int_0^z C(x,z')\mathrm{d}z'$) of light by SPM switched off.
• As the default experiment, but for the advection terms ($-u\frac{\partial P}{\partial x}$, $-w\frac{\partial P}{\partial z}$, $-u\frac{\partial N}{\partial x}$ and $-w\frac{\partial N}{\partial z}$) switched off.
Aim 2 – effect of seasonally varying incident light intensity and water temperature on bloom characteristics.
• As the default experiment, but for a constant incident light intensity $I_{in,\mathrm{const}} = 205$ μmol photons m^{-2} s^{-1}.
• As the default experiment, but for a constant water temperature $T_{\mathrm{const}} = 11$ °C

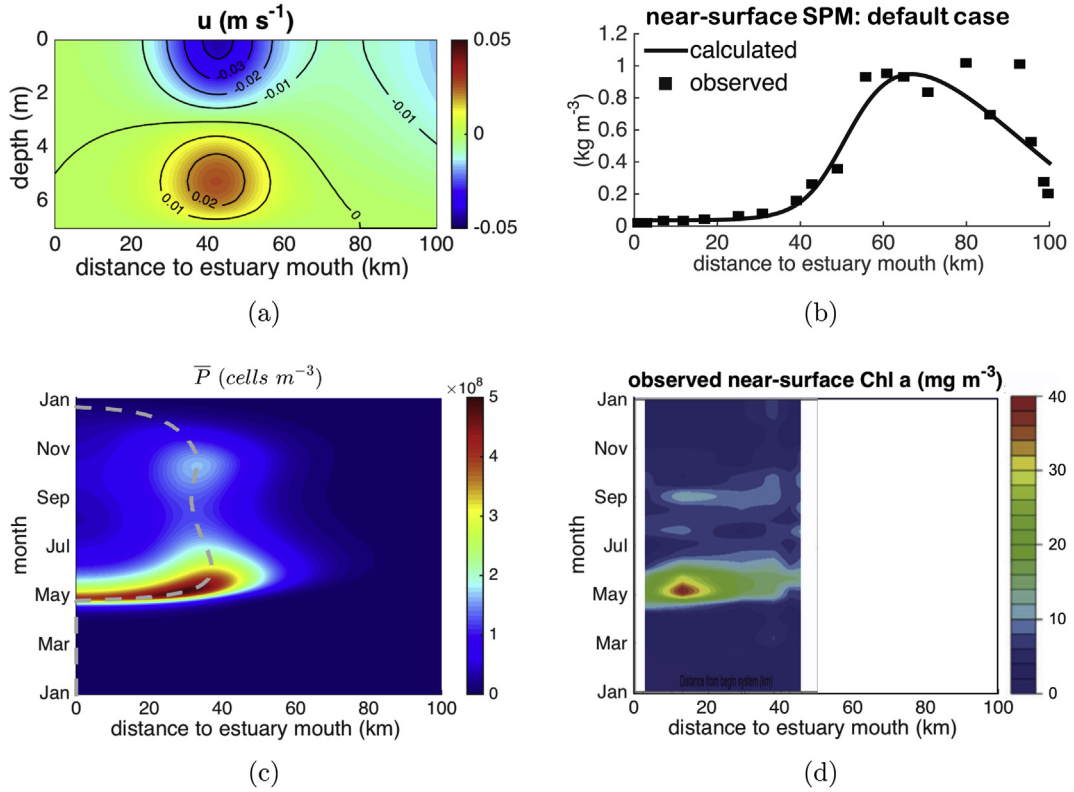

Fig. 4. Results of the default experiment. (a) Colour-contour plot of the width-averaged along-estuary subtidal current velocity u as a function of distance to the estuary mouth and depth. (b) Along-estuary distribution of the calculated (solid line) and observed (square markers, reproduced from de Jonge et al. (2014)) near-surface suspended particulate matter (SPM) concentration. (c) Colour plot of the depth-averaged phytoplankton population density $\overline{P}$ as a function of distance to the estuary mouth and time in the adjusted periodic state. The gray dashed line in Fig. 4c indicates the location of the time-dependent along-estuary maximum depth-averaged population density $\overline{P}_{max}$ in the domain. (d) Observed near-surface Chl-a concentration in the year 2013, reproduced from Brinkman et al. (2014). Here the blank regions indicate the areas in which field data are not available. Note that only a qualitative comparison between $\overline{P}$ and Chl-a pattern is made.

those in the default experiment and the bloom intensity $\overline{P}_{\text{bloom}} = 520 \cdot 10^7 \text{cells m}^{-3}$. Another notable feature is that $\overline{P}_{max}$ occurs in the area $x > 75$ km rather than in the lower reach. Thus, the light attenuation by SPM strongly affects the intensity and along-estuary location of phytoplankton blooms. Moreover, the spatiotemporal pattern of $\overline{P}$ (see Fig. 5c) shows that in the area $x > 50$ km, the bloom persists for the entire year.

If the advection terms ($-u\frac{\partial P}{\partial x}$, $-w\frac{\partial P}{\partial z}$, $-u\frac{\partial N}{\partial x}$ and $-w\frac{\partial N}{\partial z}$) are switched off, the behaviour of $\overline{P}_{max}$ is similar to that of the default experiment. However, $\overline{P}_{max}$ is smaller when advection terms are switched off. Specifically, bloom intensities $\overline{P}_{\text{bloom}} = 19 \cdot 10^7 \text{cells m}^{-3}$ and $5 \cdot 10^7 \text{cells m}^{-3}$ for the spring bloom and autumn bloom, respectively. Furthermore, the peak of the spring bloom is delayed by two weeks compared to the one in the default experiment. Moreover, the along-estuary locations of the blooms hardly differ between two experiments. Thus, advective processes due to subtidal currents have a noticeable impact on intensity, limited influence on timing and a negligible effect on along-estuary location of blooms.

3.2.2. Seasonally varying incident light intensity and water temperature

When a constant incident light intensity $I_{in,\text{const}} = 205$ μmol photons m^{-2} s^{-1} (which is the annually-averaged value of I_{in} in the default experiment) is imposed, it results in a similar $\overline{P}_{max}$ pattern compared to the one in the default experiment. However, for $I_{in,\text{const}}$, the spring bloom is less intense with $\overline{P}_{\text{bloom}} = 30 \cdot 10^7 \text{cells m}^{-3}$ and the values of $P_{s,\max}$ during January–March are at least one order of magnitude higher than those for the default experiment. The timing and the along-estuary location of the spring bloom, as well as the characteristics of the secondary bloom, hardly differ between the two experiments. Hence, the seasonally varying incident light intensity largely affects the population densities in winter - early spring and influences the intensity of the spring bloom, whereas it has marginal effect on the timing and along-estuary location of blooms.

When a constant water temperature $T_{\text{const}} = 11$ °C (which is the annual mean of T in the default experiment) is used, a marked difference from the default experiment is that only one single bloom occurs in one year. Furthermore, for T_{const}, $\overline{P}_{max}$ in winter is noticeably higher and a weaker spring bloom occurs, with $\overline{P}_{\text{bloom}} = 27 \cdot 10^7 \text{cells m}^{-3}$. Moreover, the bloom peak occurs almost seven weeks earlier compared to that of the spring bloom in the default experiment. Thus, the seasonally varying water temperature is a determining factor for the occurrence of the secondary bloom. Furthermore, it largely affects the timing of the spring bloom and influences bloom intensity, whereas it has hardly any impact on the along-estuary location of the spring bloom.

4. Discussion

In Section 4.1, the mechanisms controlling the phytoplankton bloom pattern for the default experiment are explained by quantifying the contribution of each factor to the local accumulation rate of P. Next, the results of sensitivity studies are further analysed in Section 4.2. In Section 4.3, the comparison between the modelled spatiotemporal distribution of nutrient concentration N in the default experiment and the field data is presented and discussed.

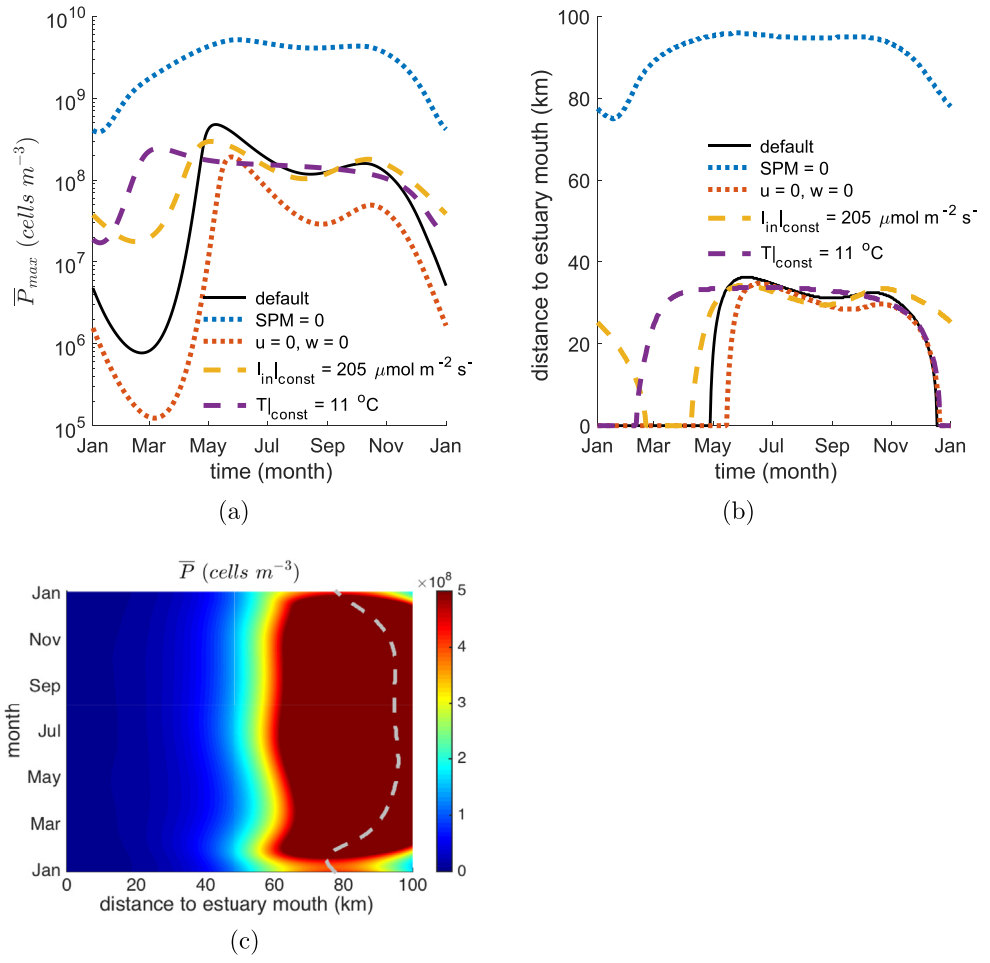

Fig. 5. (a) The along-estuary maximum depth-averaged population density $\overline{P}_{max}$ against time, which are plotted for the default experiment and for the sensitivity experiments where light attenuation ($-k_c \int_0^z C(x,z')\mathrm{d}z'$) by SPM was switched off, advection (i.e., terms $u\frac{\partial P}{\partial x}$, $w\frac{\partial P}{\partial z}$, $u\frac{\partial N}{\partial x}$ and $w\frac{\partial N}{\partial z}$) of P and N by subtidal currents was switched off, constant incident light intensity $I_{in,\mathrm{const}} = 205$ μmol photons m^{-2} s^{-1} was used and constant water temperature $T_{\mathrm{const}} = 11$ °C was imposed, respectively. (b) As (a), but for the along-estuary location χ of $\overline{P}_{max}$. (c) As Fig. 4c, but for the light attenuation by SPM switched off.

Finally, the consequences of several assumptions in the model are discussed (Section 4.4).

4.1. Mechanisms underlying bloom dynamics

The equation governing phytoplankton dynamics (Eq. (2)) is rewritten as

$$\underbrace{\frac{1}{P}\frac{\partial P}{\partial t}}_{\text{total accumulation rate}} = \underbrace{(\mu - m)}_{\text{net specific growth rate}} + \underbrace{\frac{1}{P}\left[-v\frac{\partial P}{\partial z} - w\frac{\partial P}{\partial z} - u\frac{\partial P}{\partial x} + \frac{\partial}{\partial z}\left(\kappa_v\frac{\partial P}{\partial z}\right) + \frac{1}{b}\frac{\partial}{\partial x}\left(b\kappa_h\frac{\partial P}{\partial x}\right)\right]}_{\text{accumulation rate due to non-local processes}}. \quad (16)$$

Here, the left-hand side term is the total accumulation rate of P at a fixed position, which is a summation of net specific growth rate and accumulation rate due to non-local processes. The latter results from sinking, along-estuary and vertical advection, along-estuary and vertical mixing.

Since P is vertically almost uniform, in the first step toward understanding results, the depth-averaged values of the net specific growth rate $\overline{(\mu - m)} = \frac{1}{H}\int_0^H (\mu - m)\,\mathrm{d}z$, as well as those of the accumulation rate due to non-local processes are calculated for the default experiment. The resultant spatiotemporal patterns are shown in Fig. 6a and b. Clearly, in the lower reach $x < 40$ km where blooms are found, $\overline{(\mu - m)}$ has high values whilst the accumulation rates due to non-local processes are low. These findings suggest that in the example estuary, bloom dynamics is primarily controlled by local net growth and the role of non-local processes is mainly to transport phytoplankton produced in the lower reach to the middle and upper reach.

To further analyse the behaviour of $\overline{(\mu - m)}$, the area of nutrient-limited growth (defined in Section 2.1.2) has been indicated in Fig. 6a. Note that here nutrient/light limitation is determined by the depth-averaged limitation index (see Table 3). Since the loss rate m in this experiment is constant in both space and time, changes in $\overline{(\mu - m)}$ are due to variations in the specific growth rate μ. In January–February, $\overline{(\mu - m)}$ is negative due to low incident light intensities I_{in} and low water temperature T. As a result, $\overline{P}$ is low, as is shown in Fig 6d. From March on, as I_{in} and T increase, $\overline{(\mu - m)}$ rapidly increases, which leads to the formation of the spring bloom in the lower reach.

During the spring bloom, high density of phytoplankton quickly

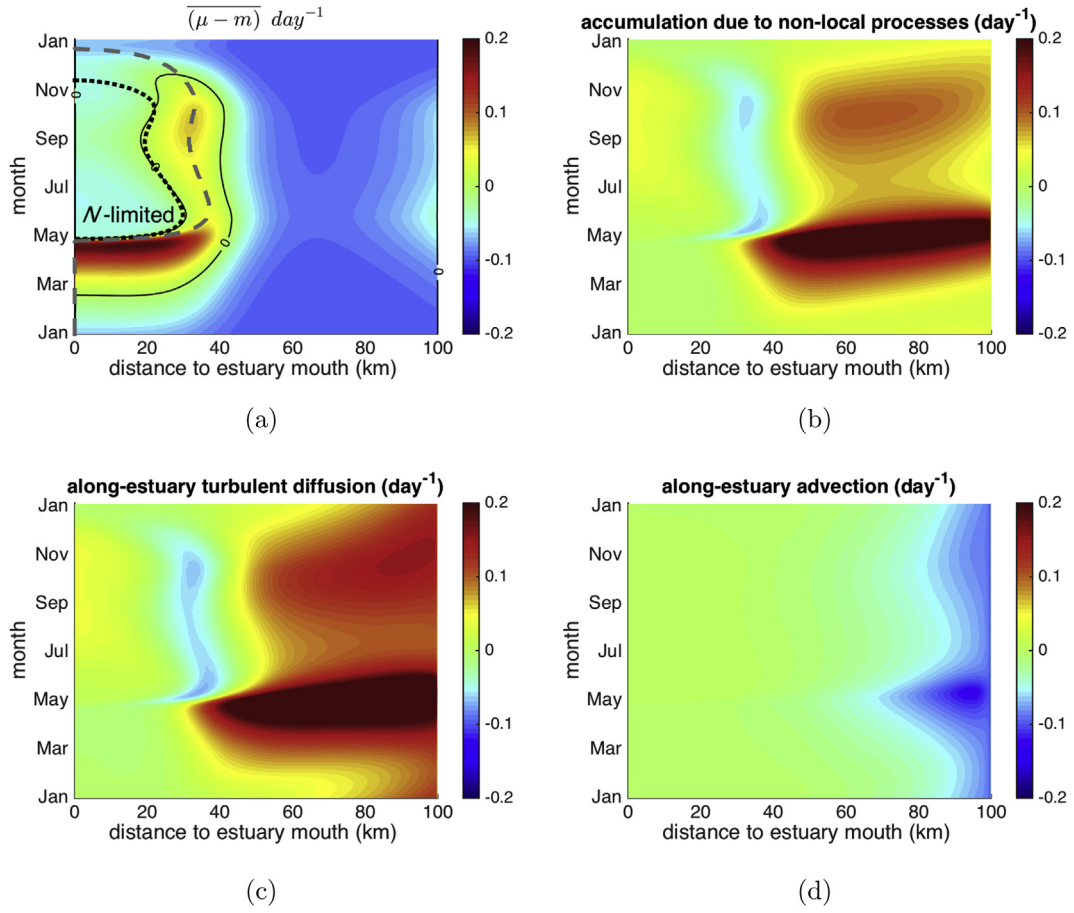

Fig. 6. (a) Colour plot of the depth-averaged net specific growth rate $\overline{(\mu - m)}$ as a function of distance to the estuary mouth and time for the default experiment. The black dotted lines indicate the transition between areas of nutrient and light limitation, and the gray dashed lines show the location of the along-estuary maximum depth-averaged population density $\overline{P}_{max}$. (b), (c) and (d): As (a), but for the depth-averaged values of the accumulation rates due to non-local processes, due to along-estuary turbulent diffusion $\overline{\frac{1}{Pb}\frac{\partial}{\partial x}\left(b\kappa_h\frac{\partial P}{\partial x}\right)}$ and due to along-estuary advection $\overline{-\frac{u}{P}\frac{\partial P}{\partial x}}$, respectively.

Table 3
Symbols that are used for presenting and discussing model results.

Symbol	Definition
$\overline{P}_{max}$	the time-dependent along-estuary maximum depth-averaged population density
$\overline{P}_{\text{bloom}}$	the intensity of a bloom, which is quantified by the local maxima of $\overline{P}_{max}$
χ	the longitudinal distance from the estuary mouth to the site of $\overline{P}_{max}$
$\overline{(\mu - m)}$	the depth-averaged net specific growth rate, viz., $\overline{(\mu - m)} = \frac{1}{H}\int_0^H (\mu - m)\,\mathrm{d}z$
$\overline{(\mu - m)}\|_{x=\chi}$	the depth-averaged net specific growth rate at location χ
$\left(\frac{N}{H_N+N} - \frac{I}{H_I+I}\right)$	limitation index, negative (positive) values indicate nutrient- (light-)limited growth
$\overline{\left(\frac{N}{H_N+N} - \frac{I}{H_I+I}\right)}$	depth-averaged limitation index, i.e., $\overline{\left(\frac{N}{H_N+N} - \frac{I}{H_I+I}\right)} = \frac{1}{H}\int_0^H \left(\frac{N}{H_N+N} - \frac{I}{H_I+I}\right)\mathrm{d}z$

depletes large amount of nutrient. Consequently, the region of large $\overline{(\mu - m)}$ shrinks to a narrow area away from the estuary mouth (Fig. 6a), which results in an upstream shift of the bloom location (Fig. 4c). Nutrient limitation eventually terminates of the spring bloom, as is evident by the fact that in the lower reach $\overline{(\mu - m)}$ drops below zero in the area of nutrient limitation. Such alternation of limitation factors, that is, light-limited growth in winter - early spring and nutrient-limited growth in late spring - summer, has also been reported in other temperate estuaries, such as the Delaware estuary (USA) (Pennock and Sharp, 1994) and the Colne Estuary (UK) (Kocum et al., 2002).

In late May, the values of $\overline{(\mu - m)}$ start to decrease (Fig. 6a) when T is above the optimum temperature $T_{opt} = 15\,^{\circ}\mathrm{C}$ for phytoplankton growth, which accelerates the termination of the spring bloom. From August on, $\overline{(\mu - m)}$ increases again as T approaches the optimum temperature T_{opt}, which triggers the secondary bloom in a narrow area seaward of the estuary mouth (Fig. 4c), where nutrient concentrations are relatively high.

Comparison of the terms that contribute to the non-local accumulation reveals that the along-estuary turbulent diffusion (see Fig. 6c) dominates, which smoothes the longitudinal gradient of P induced by along-estuary variation of $\overline{(\mu - m)}$. The along-

estuary advection of P, as is shown in Fig. 6d, only has noticeable contribution in the vicinity of the river head, where river flow velocities (see Fig. 4a) are large due to small estuary width. Since the upper reach is unproductive, the along-estuary advection of P has little influence on phytoplankton blooms. However, the along-estuary advection of nutrient N is essential for nutrient availability in the entire domain, as is demonstrated in Electronic Supplement 1. Specifically, river flow is the main forcing agent that drives the seaward transport of nutrient in the upper and middle reaches from its riverine source. Finally, sinking, vertical advection and vertical turbulent diffusion give little contributions (less than $0.06 day^{-1}$) to the total accumulation rate of P.

4.2. Sensitivity experiments

In this section, the behaviour of depth-averaged net specific growth rate $\overline{(\mu - m)}$ is examined to analyse the bloom evolution in each sensitivity experiment. To facilitate comparison among sensitivity experiments, the temporal evolution of the depth-averaged net specific growth rate $\overline{(\mu - m)}|_{x=\chi}$ (see Table 3, here χ is the longitudinal distance from the estuary mouth to the site where $\overline{P}_{max}$ is found) at location χ is presented.

4.2.1. Light attenuation by SPM and advection by subtidal current

When the light attenuation by SPM is switched off, in the middle and upper reaches ($x > 40$ km), light penetrates much further into the water column. As a result, positive net growth is possible in these areas, as is shown in Fig. 7a. The critical role of light attenuation by SPM on the along-estuary distribution of phytoplankton biomass (growth) has also been found for the Delaware estuary by McSweeney et al. (2016), who conducted simulations under constant incident light intensity. The landward shift of the productive area further allows higher rates of nutrient supply to phytoplankton due to decreased distance between the area of high population densities and the river head (where nutrient enters the estuary). Thus, $\overline{(\mu - m)}$ in the area $x > 90$ km is generally high throughout the year. As a result, a long-lasting, intense bloom occurs, as is shown in Fig. 5a and b. Close to the river head, high population densities lead to consumption of large amount of nutrient, which results in that in the area $x < 80$ km nutrient limitation exists for most of the year. Consequently, in the lower reach, values of $\overline{P}_{max}$ are relatively low (Fig. 5c). In the area $50 < x < 80$ km, the high population densities are due to the along-estuary advection and turbulent diffusion (results not shown) of phytoplankton from the highly productive area close to the river head.

If the advection terms are switched off, the values of N (results not shown) in the entire estuary are lower than those of the default experiment. This is because the along-estuary advection of N by subtidal current is essential for the seaward transport of nutrient in the upper and middle reaches from its riverine source (see Electronic Supplement 1). Since nutrient availability sets the potential phytoplankton production, population densities (Fig. 5a) are lower when the advection terms are switched off. This explains why field studies (for instance, de Jonge and Essink, 1991) reveal a positive relation between phytoplankton production and river discharge. Moreover, as is illustrated by the temporal evolution of the depth-averaged net specific growth rate $\overline{(\mu - m)}|_{x=\chi}$ (see Fig. 7b), under lower nutrient availability positive net growth of phytoplankton occurs later. This, together with a lower population density (Fig. 5a) in winter and early spring, leads to a later spring bloom than that in the default experiment.

4.2.2. Seasonally varying incident light intensity and water temperature

If a constant incident light intensity $I_{in,\mathrm{const}} = 205\ \mu$ mol photons $m^{-2}\ s^{-1}$ is imposed, then $\overline{(\mu - m)}|_{x=\chi}$ (see Fig. 7b) in winter is larger than that of the default experiment, in which I_{in} has a seasonal cycle. As a result, $\overline{P}$ in winter is higher for $I_{in,\mathrm{const}}$ and it takes less time to form a spring bloom, as is shown in Fig. 5a. The high population density of phytoplankton in winter quickly consumes nutrient, thereby causing nutrient limitation to occur already in January (results not shown). Thus, in March–April, $\overline{(\mu - m)}|_{x=\chi}$ is much lower than that of the default experiment, and the spring bloom is therefore less intense.

When a constant water temperature $T_{\mathrm{const}} = 11\ ^{\circ}$C is imposed, the maximum growth rate $\mu_T = 2.1\ day^{-1}$ of phytoplankton is high throughout the year. Consequently, for T_{const}, positive values of $\overline{(\mu - m)}|_{x=\chi}$ (see Fig. 7b) occurs much earlier than that in the default

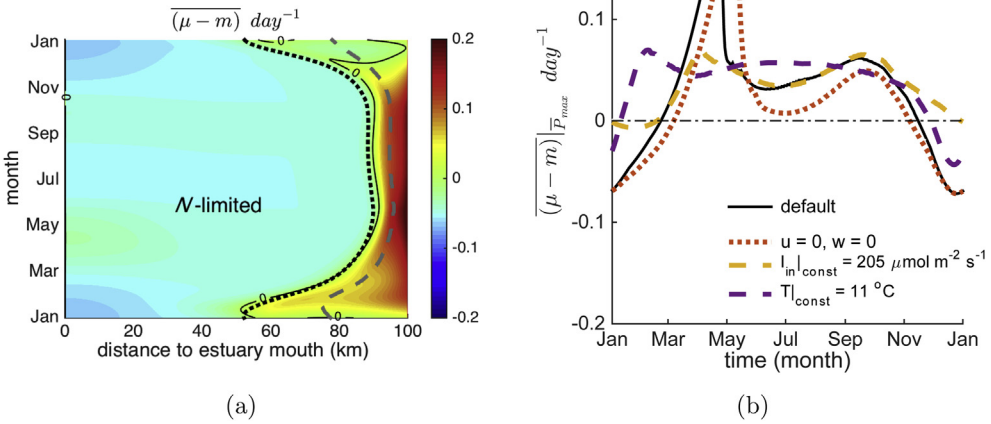

Fig. 7. (a) As Fig. 6a (colour plot of the depth-averaged net specific growth rate), but for the light attenuation ($-k_c \int_0^z C(x,z')dz'$) by SPM switched off. (b) The net specific growth rates $\overline{(\mu - m)}|_{x=\chi}$ against time, which are plotted for the default experiment and for the sensitivity experiments where light attenuation by SPM was switched off, advection (i.e., terms $u\frac{\partial P}{\partial x}$, $w\frac{\partial P}{\partial z}$, $u\frac{\partial N}{\partial x}$ and $w\frac{\partial N}{\partial z}$) of P and N by subtidal currents was switched off, constant incident light intensity $I_{in,\mathrm{const}} = 205\ \mu$mol photons $m^{-2}\ s^{-1}$ was used and constant water temperature $T_{\mathrm{const}} = 11\ ^{\circ}$C was imposed, respectively. Here, χ is the longitudinal distance from the estuary mouth to the site of $\overline{P}_{max}$. The black dash-dot line indicates zero.

experiment. As a result, population densities (Fig. 5a) for T_{const} are high in winter and they increase rapidly with time, which leads to a bloom in early spring. The consumption of nutrient by the large amount of phytoplanktkon results in generally lower N values and a less intense spring bloom compared to the default experiment. Because of nutrient limitation, $\overline{(\mu - m)}|_{x=\chi}$ slightly decreases during the bloom (in February–March). Since in this experiment the growth rate does not depend on water temperature, in April–June, $\overline{(\mu - m)}|_{x=\chi}$ keeps increasing with the increasing incident light intensity I_{in} until the end of June. The decay of the spring bloom for T_{const} is therefore slower than that in the default experiment. From July on, the specific growth rate decreases monotonously with I_{in} and no secondary bloom occurs for T_{const}. This agrees with the finding of Naithani et al. (2016) that a parameterisation of μ_T that accounts for an optimum temperature for phytoplankton growth is needed for reproducing the spring and autumn blooms in the Scheldt estuary.

The finding in this study that seasonally varying water temperature has larger impact on timing of spring blooms than seasonally varying incident light intensity deviates from the view on phytoplankton dynamics in open ocean and shelf sea that spring blooms are triggered by seasonal increases in light intensity (Sverdrup, 1953; Riley, 1967). This is caused by the differences between estuarine and open water conditions. First, in deep-water marine systems, increased solar radiation in spring heats up the upper water column, which therefore results in vertical stratification and leads to a shallower mixing layer that allows spring blooms to develop. However, in shallow, vertically well-mixed estuaries, vertical mixing is intense throughout the entire water column and the mixing depth is equivalent to the water depth. Second, the specific growth rate increases more effectively with rising water temperature. For coastal waters and oceans, water temperature shows less temporal variability compared to that of the much shallower estuarine systems.

4.2.3. Additional sensitivity experiments

Results of additional sensitivity experiments (see Electronic Supplement 1) reveal that the setting of boundary conditions, initial conditions, as well as the values of biological parameters have only moderate quantitative impacts on the timing, intensity or along-estuary location of phytoplankton blooms, but they do not affect the overall findings of the previous sections.

As was discussed in Section 4.1, a decrease of the depth-averaged net specific growth rate $\overline{(\mu - m)}$ during the summer season followed by an increase of $\overline{(\mu - m)}$ in early autumn causes the occurrence of the autumn bloom. In the exploratory model, such changes in $\overline{(\mu - m)}$ values are induced by the presence of an optimum temperature T_{opt} for the gross growth of phytoplankton, which is lower than the maximum water temperature. If the value of T_{opt} approaches the maximum water temperature, the secondary autumn bloom merges with the spring bloom, as is shown in Fig. S6 in Electronic Supplement 1. This is because the values of $\overline{(\mu - m)}$ are higher for larger T_{opt} in summer season, which leads to larger nutrient consumption. Thus, after the spring bloom, the values of the population density are high throughout the summer and no autumn bloom occurs.

The decrease of $\overline{(\mu - m)}$ during summer could also be caused by an increased grazing rate, as is discussed below. Further experiments were conducted to examine the impact of seasonally varying loss rate on the characteristics of blooms. One experiment was carried out, in which the seasonally-varying water temperature was switched off by using a constant $T_{const} = 11\ ^{\circ}C$ and the loss of phytoplankton by microzooplankton grazing was accounted for. The latter has been suggested to significantly contribute to the loss of phytoplankton during late spring and summer seasons (Loebl and van Beusekom, 2008). Specifically, a time-dependent loss rate m_τ was used, which reads

$$m_\tau = \begin{cases} m_0 + 0.5\, m_g \left[1 - \cos\left(2\pi\, \dfrac{\tau - \tau_1}{\tau_2 - \tau_1}\right)\right] & \tau_1 < \tau < \tau_2 \\ m_0 & 0 < \tau < \tau_1 \text{ or } \tau_2 < \tau < T_y \end{cases} \tag{17}$$

In this expression, τ is the day number in a year, starting from January 1st, and τ_1 and τ_2 are the day numbers, between which the grazing of phytoplankton by microzooplankton occurs. Parameter m_0 is the basic loss rate, which is taken the same value ($0.1\ day^{-1}$) as the constant loss rate in the default experiment, and m_g is the maximum grazing rate. Here $\tau_1 = 135$ day (mid May) and $\tau_2 = 270$ day (end of September) were chosen based on field data of Loebl and van Beusekom (2008). Furthermore, $m_g = 0.1\ day^{-1}$ was used. The temporal variation of m_τ is illustrated in Fig. 8a.

Next, the seasonally-varying water temperature was switched on and three experiments were carried out with $m_g = 0.1,\ 0.2,$ and $0.4\ day^{-1}$, respectively. The last experiment also used the seasonally-varying water temperature and it employed the parameterisation of loss rate used by Arndt et al. (2007) (hereafter referred to as m_{A07}, see their Eqs. (30) and (31)). In the above cited study, m_{A07} accounts for the combined effects of cell lysis and grazing by higher trophic levels in the Scheldt estuary. The temporal variation of m_{A07} is shown in Fig. 8a. The time-dependent along-estuary maximum depth averaged population density $\overline{P}_{max}$ for these five experiments and for the default experiment is shown in Fig. 8b, c and 8d.

As is discussed in Section 4.2.2, when the seasonally-varying water temperature is switched off, the autumn bloom does not occur anymore due to the monotonous decrease of the specific growth rate since July. Now if m_τ is used, the autumn bloom forms (see Fig. 8b). This is because the net specific growth rate decreases in the summer season and it increases again in the autumn due to the temporal variation of grazing rate.

When the seasonally-varying water temperature is switched on and m_τ is used, the gross features of the blooms are identical to those of the default experiment, that is, a spring bloom occurs in the lower reach, followed by a secondary autumn bloom (see Fig. 8c). In particular, the timing, intensity and along-estuary location of the spring bloom are hardly affected. This is because the grazing of phytoplankton by microzooplankton is included after the peak of the spring bloom (early May). However, noticeable quantitative differences exists in P patterns during summer and autumn seasons. Specifically, the population density is lower than that of the default experiment due to the increased loss rate. As a result, when a larger value of m_τ is used, it takes more time to form an autumn bloom and therefore the autumn bloom is significantly delayed. Furthermore, the intensity of the autumn bloom significantly decreases when the grazing rate is larger than $0.4\ day^{-1}$.

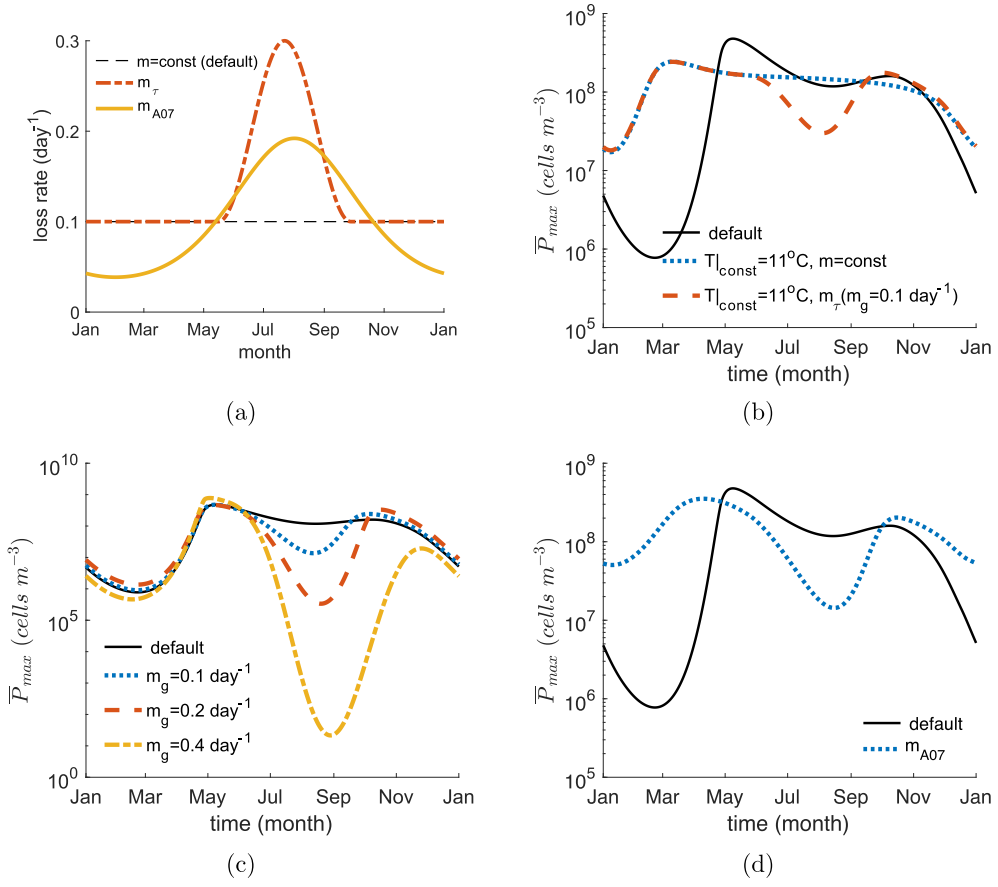

Fig. 8. (a): The loss rate of phytoplankton against time for different parameterisations. The blue dash-dotted line (m_τ) is calculated by Eq. (17), which accounts for the grazing rate of phytoplankton by microzooplankton. The red solid line follows the parameterisation (m_{A07}) of loss rate in Arndt et al. (2007). The black dashed line indicates the constant loss rate used in the default experiment of this study. (b): As Fig. 5a, but for the experiments in which constant water temperature $T_{const} = 11\ ^\circ C$ was imposed and both $T_{const} = 11\ ^\circ C$ and a time-dependent loss rate m_τ (see Eq. (17), here $m_g = 0.1\ day^{-1}$) were imposed. (c): As Fig. 5a, but for three experiments in which both seasonally varying water temperature and m_τ were used and $m_g = 0.1,\ 0.2,$ and $0.4\ day^{-1}$, respectively. (d): As Fig. 5a, but for m_{A07}.

If m_{A07} is used, the gross features of blooms remain unchanged with respect to those of the default experiment, although quantitative differences exist. In the winter and early spring, population density is larger for m_{A07} due to lower loss rates than that in the default expeirment. The resultant higher net specific growth rate in this period results in an earlier and less intense spring bloom. In summer, the population density is lower when m_{A07} is used due to high loss rates.

4.3. Spatiotemporal distribution of N in the default experiment

Fig. 9a shows the spatiotemporal behaviour of the depth-averaged nutrient concentration $\overline{N}$ for one year in the adjusted periodic state of the default experiment. Overall, the pattern of $\overline{N}$ has characteristics that are also observed in the field, such as decreasing values towards the estuary mouth. In winter and spring (before early April), in the lower reach (seaward of 40 km) $\overline{N}$ noticeably increases with time because the amount of the nutrient uptake by phytoplankton is small because of low P values during this period. Afterwards, during the spring bloom (see Fig. 4c) in late April–June, $\overline{N}$ rapidly drops due to the uptake by large amounts of phytoplankton during the spring bloom.

Observed nutrient patterns (see Fig. 9b for phosphorus and Fig. 9c for silicon) in the Ems estuary shows similar characteristics. However, there are several characteristics of the field data that are not captured by the model. These differences in the gross features occur because the present exploratory model only includes a limited number of processes, following Huisman et al. (2006). Examples of aspects that affect nutrient dynamics and that are not accounted for are adsorption/desorption processes, the seasonally varying riverine nutrient input, the switch of limiting nutrients (e.g. from phosphorus to silicon, as is suggested by Fig. 9b and c, the upstream transport and remineralisation of marine particulate organic matter.

4.4. Model assumptions and consequences

4.4.1. Intratidal processes

Accounting for tides introduces along-estuary transport of SPM, phytoplankton and nutrient by additional subtidal current components (such as flow induced by internal tidal asymmetry) and by tidal pumping. Both model and field studies (Burchard et al., 2013; Becherer et al., 2016) have demonstrated that tidal pumping is effective in transporting SPM. In the present model, these tidal effects on SPM distribution have been implicitly accounted for via the input parameter θ. It would be interesting to explicitly model the above-mentioned intratidal processes in near future.

4.4.2. Magnitude and vertical shape of A_v and κ_v

Within the turbidity zones, large vertical gradients in SPM concentration (see Talke et al., 2009b) may induce strong density stratification. In these areas, net pelagic phytoplankton growth is

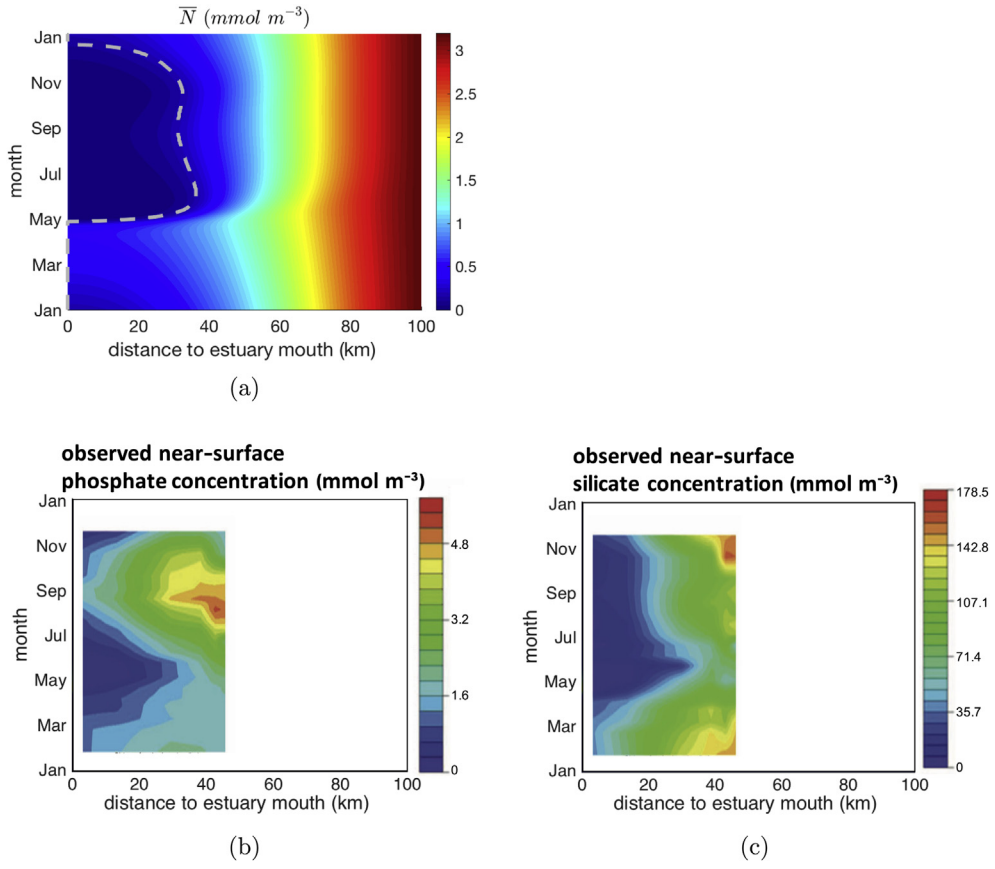

Fig. 9. (a): Colour plot of the depth-averaged nutrient concentration $\overline{N}$ as a function of the distance to the estuary mouth and time in the adjusted periodic state for the default experiment. (b) and (c): Observed near-surface phosphate (i.e., reactive phosphorus) and silicate (i.e., reactive silicon) concentration, respectively, in the year 2013 in the Ems estuary, reproduced from Brinkman et al. (2014). The blank regions indicate the areas in which field data are not available.

not expected because of strong light limitation. Hence, for this study, it is unlikely that accounting for along-estuary constant mixing coefficients (A_v and κ_v) will significantly affect the bloom dynamics. However, if vertical density stratification is significant, suppressed vertical mixing prevents particulate matter from being resuspended into the surface layer, thus providing light conditions favourable for phytoplankton growth (McSweeney et al., 2016). Furthermore, changes in vertical density stratification will also affect vertical mixing and subtidal currents and therefore influence distributions of P (Liu and de Swart, 2017). Thus, in such circumstances, the magnitudes and vertical shapes of A_v and κ_v should be estimated based on local vertical density stratification.

4.4.3. Flocculation and hindered settling of SPM

The settling velocity of SPM was also kept constant in both time and space in this study, and the flocculation and hindered settling of SPM are therefore not accounted for. This assumption has been widely used by previous exploratory studies that were applied to highly turbid estuaries (e.g. Talke et al., 2009b; Chernetsky et al., 2010; Kumar et al., 2017), in which model results successfully capture the gross features of observed SPM distributions. Nevertheless, if the detailed spatiotemporal distributions of P and SPM are required, flocculation and hindered settling of SPM should be considered.

4.4.4. Seasonal variation of river discharge

Temporal variability in river discharge will affect nutrient transport and therefore the characteristics of phytoplankton blooms. Moreover, variations in river discharge causes changes in the spatiotemporal pattern of SPM (Arndt et al., 2007). Thus, for further understanding of detailed (short-term) spatiotemporal behaviour of phytoplankton blooms, time-dependent river discharge should be accounted for.

4.4.5. Variable topography

Changes in water depth affect the depth-averaged net specific growth rate of phytoplankton and thereby the characteristics of blooms (Liu and de Swart, 2015). Furthermore, conditions of vertical mixing, distributions of subtidal currents and SPM are also dependent on water depth. For instance, May et al. (2003) have found that accounting for lateral variation in topography is important for modelling phytoplankton dynamics since behaviour of both P and SPM in shallow waters has a significant impact on phytoplankton and SPM dynamics of the whole estuarine system. For estuaries that comprise deep channels and tidal flats, microphytobenthos significantly contribute to primary production in turbidity zones (de Jonge and van Beusekom, 1992; Irigoien and Castel, 1997). The effect of variable bottom topography on phytoplankton dynamics is an important topic to be investigated in the future.

4.4.6. Multiple nutrients

In this study, phosphorus was accounted for as the limiting nutrient based on the field data of Brinkman et al. (2014). However, silicon limitation on diatom growth has also been reported in other years (e.g. 2012, based on the same study cited above) in the Ems estuary and in other estuaries (for instance, the Scheldt estuary, according to Arndt et al., 2007). Moreover, it has been reported that

in many estuaries, the limiting nutrient switches from phosphorus (or silicon) in spring to nitrogen in summer (Pennock and Sharp, 1994). Mechanisms dominating biogeochemical processes differ among different nutrients, which alter the relative availability of these nutrients (Howarth, 1988). Thus, it is interesting to consider phytoplankton bloom dynamics that are subject to multiple limiting nutrients in future studies.

5. Conclusions

This study focuses on gaining fundamental insight into the mechanisms underlying phytoplankton dynamics in turbid, well-mixed, temperate estuaries. Specifically, the quantitative effect of following two combinations of dependent control factors on phytoplankton blooms is investigated: 1) SPM distribution and subtidal current, and 2) seasonally varying incident light intensity and water temperature. The novel aspect of this study is that using an exploratory model, the impact of the above-mentioned dependent aspects on bloom dynamics is quantified in isolation. The model was able to capture the gross features of the observed phytoplankton blooms in the Ems estuary in 2013, i.e., in the lower reach a spring bloom occurs, which is followed by a secondary bloom in autumn. The bloom characteristics, i.e. timings, intensities and along-estuary locations of blooms, are determined by local net growth of phytoplankton.

Sensitivity experiments suggest that the along-estuary distribution of suspended particulate matter (SPM) concentration is a determining factor for the along-estuary locations of blooms, i.e., the blooms are restricted to the lower reach where SPM concentrations are relatively low, and it also affects the bloom intensities by controlling the distance between bloom locations and the river head, where nutrients enter the estuary. The advection of nutrients influence the bloom intensities by regulating the seaward transport of nutrient. In this model, the seasonally varying water temperature has a larger impact on the timing of spring blooms than the seasonally varying incident light intensity. This is because the specific growth rate increases more effectively with rising water temperature. Within the framework of the exploratory model, the occurrence of an autumn bloom is due to the fact that during the summer season, the net specific growth rate of phytoplankton decreases. The latter is likely to result from an optimum water temperature (smaller than maximum water temperature) for phytoplankton growth. Note that seasonal variations in other aspects, for instance, loss of phytoplankton due to grazing also affect the occurrence and characteristics of autumn blooms.

Acknowledgments

The first author is financially supported by the China Scholarship Council [NO. 201206250039].

Appendix A. Supplementary data

Supplementary data related to this article can be found at https://doi.org/10.1016/j.ecss.2018.01.010

References

Arndt, S., Vanderborght, J.-P., Regnier, P., 2007. Diatom growth response to physical forcing in a macro tidal estuary: coupling hydrodynamics, sediment transport, and biogeochemistry. J. Geophys. Res. 112 https://doi.org/10.1029/2006JC003,581. C05,045.

Becherer, J., Flöser, G., Umlauf, L., Burchard, H., 2016. Estuarine circulation versus tidal pumping: sediment transport in a well-mixed tidal inlet. J. Geophys. Res.: Oceans 121, 6251–6270.

van Beusekom, J.E.E., de Jonge, V.N., 1998. Retention of phosphorus and nitrogen in the Ems estuary. Estuaries 21, 527–539.

Brinkman, A.G., Riegman, R., Jacobs, P., Khn, S., Meijboom, A., 2014. Ems-dollard Primary Production Research, Full Data Report. Tech. Rep. C160/14, IMARES.

Brussaard, C.P.D., 2004. Viral control of phytoplankton populationsa review. J. Eukaryot. Microbiol. 51, 125–138.

Burchard, H., Schuttelaars, H.M., Geyer, W.R., 2013. Residual sediment fluxes in weakly-to-periodically stratified estuaries and tidal inlets. J. Phys. Oceanogr. 43, 1841–1861.

Butterwick, C., Heaney, S.I., Talling, J.F., 2005. Diversity in the influence of temperature on the growth rates of freshwater algae, and its ecological relevance. J. Freshw. Biol. 50, 291–300.

Camacho, R.A., Martin, J.L., Paul, M.J., Stribling, J., 2015. Modeling the factors controlling phytoplankton in the St. Louis Bay estuary, Mississippi and evaluating estuarine responses to nutrient load modification. J. Environ. Eng. 141, 04014,067.

Chernetsky, A., Schuttelaars, H.M., Talke, S.A., 2010. The effect of tidal asymmetry and temporal settling lag on sediment trapping in tidal estuaries. Ocean Dynam. 60, 1219–1241.

Cira, E.K., Paerl, H.W., Wetz, M.S., 2016. Effects of nitrogen availability and form on phytoplankton growth in a eutrophied estuary (Neuse River Estuary, NC, USA). PLoS One 11. https://doi.org/10.1371/journal.pone.0160,663.

Cloern, J.E., Foster, S.Q., Kleckner, A.E., 2014. Phytoplankton primary production in the world's estuarine-coastal ecosystems. Biogeosciences 11, 2477–2501.

Colijn, F., 1982. Light absorption in the waters of the Ems-Dollard estuary and its consequences for the growth of phytoplankton and microphytobenthos. Neth. J. Sea Res. 15, 196–216.

Colijn, F., 1983. Primary Production in the Ems-dollard Estuary. University of Groningen, The Netherlands. PhD thesis.

Domingues, R.B., Guerra, C.C., Barbosa, A.B., Galvão, H.M., 2017. Will nutrient and light limitation prevent eutrophication in an anthropogenically-impacted coastal lagoon? Continent. Shelf Res. 141, 11–25.

Eppley, R.W., 1972. Temperature and phytoplankton growth in the sea. Fish. Bull. 70, 1063–1085.

Godhe, A., Asplund, M.E., Härnström, K., Saravanan, V., Tyagi, A., Karunasagar, I., 2008. Quantification of diatom and dinoflagellate biomasses in coastal marine seawater samples by real-time PCR. Appl. Environ. Microbiol. 74, 7174–7182.

Howarth, R.W., 1988. Nutrient limitation of net primary production in marine ecosystems. Annu. Rev. Ecol. Evol. Syst. 19, 89–110.

Huisman, J., Thi, N.N.P., Karl, D.M., Sommeijer, B., 2006. Reduced mixing generates oscillations and chaos in the oceanic deep chlorophyll maximum. Nature 439, 322–326.

Irigoien, X., Castel, J., 1997. Light limitation and distribution of chlorophyll pigments in a highly turbid estuary: the Gironde (SW France). Estuar. Coast Shelf Sci. 44, 507–517.

de Jonge, V.N., 1980. Fluctuations in the organic carbon to chlorophyll-a ratios for estuarine benthic diatom populations. Mar. Ecol. Prog. Ser. 2, 345–353.

de Jonge, V.N., 1983. Relations between annual dredging activities, suspended matter concentrations, and the development of the tidal regime in the Ems Estuary. Can. J. Fish. Aquat. Sci. 40, 289–300.

de Jonge, V.N., 2000. Importance of temporal and spatial scales in applying biological and physical process knowledge in coastal management, an example for the Ems estuary. Continent. Shelf Res. 20, 1655–1686.

de Jonge, V.N., van Beusekom, J.E.E., 1992. Contribution of resuspended microphytobenthos to total phytoplankton in the Ems estuary and its possible role for grazers. Neth. J. Sea Res. 30, 91–105.

de Jonge, V.N., Essink, K., 1991. Long-term changes in nutrient loads and primary and secondary production in the Dutch Wadden Sea. In: Elliott, M., Ducrotoy, J. (Eds.), Estuaries and Coasts: Spatial and Temporal Intercomparisons. Olsen&Olsen, New York, pp. 307–316.

de Jonge, V.N., de Boer, W.F., de Jong, D.J., Brauer, V.S., 2012. Long-term mean annual microphytobenthos chlorophyll a variation correlates with air temperature. Mar. Ecol. Prog. Ser. 468, 43–56.

de Jonge, V.N., Schuttelaars, H.M., van Beusekom, J.E.E., Talke, S.A., de Swart, H.E., 2014. The influence of channel deepening on estuarine turbidity levels and dynamics, as exemplified by the ems estuary. Estuar. Coast Shelf Sci. 139, 46–59.

Kocum, E., Underwood, G.J.C., Nedwell, D.B., 2002. Simultaneous measurement of phytoplanktonic primary production, nutrient and light availability along a turbid, eutrophic UK east coast estuary (the Colne Estuary). MEPS (Mar. Ecol. Prog. Ser.) 231, 1–12.

Kumar, M., Schuttelaars, H.M., Roos, P.C., 2017. Three-dimensional semi-idealized model for estuarine turbidity maxima in tidally dominated estuaries. Ocean Model. 113, 1–21.

Lionard, M., Azémar, F., Boulêtreau, Muylaert, K., Tackx, M., Vyverman, W., 2005. Grazing by meso- and microzooplankton on phytoplankton in the upper reaches of the Schelde estuary (Belgium/The Netherlands). Estuar. Coast Shelf Sci. 79, 694–700.

Liu, B., de Swart, H.E., 2015. Impact of river discharge on phytoplankton bloom dynamics in eutrophic estuaries: a model study. J. Mar. Syst. 152, 64–74.

Liu, B., de Swart, H.E., 2017. Quantifying the effect of salinity stratification on phytoplankton population density patterns in estuaries. Estuar. Coast. https://doi.org/10.1007/s12237-017-0276-4.

Loebl, M., van Beusekom, J.E.E., 2008. Seasonality of microzooplankton grazing in the northern wadden sea. J. Sea Res. 59, 203–216.

Lopes, J.F., Vaz, N., Vaz, L., Ferreira, J.A., Dias, J.M., 2015. Assessing the state of the lower level of the trophic web of a temperate lagoon, in situations of light or

nutrient stress: a modeling study. Ecol. Model. 313, 59–76.
Lucas, L.V., Koseff, J.R., Monismith, S.G., Cloern, J.E., Thompson, J.K., 1999. Processes governing phytoplankton blooms in estuaries. ii: the role of horizontal transport. Mar. Ecol. Prog. Ser. 187, 17–30.
Luo, L., Wang, J., Schwab, D.J., Vanderploeg, H., Leshkevich, G., Bai, X., Hu, H., Wang, D., 2012. Simulating the 1998 spring bloom in Lake Michigan using a coupled physical-biological model. J. Geophys. Res. 117 https://doi.org/10.1029/2012JC008,216.
van Maren, D.S., van Kessel, T., Cronin, K., Sittoni, L., 2015. The impact of channel deepening and dredging on estuarine sediment concentration. Continent. Shelf Res. 95, 1–14.
May, C.L., Koseff, J.R., Lucas, L.V., Cloern, J.E., Schoellhamer, D.H., 2003. Effects of spatial and temporal variability of turbidity on phytoplankton blooms. Mar. Ecol. Prog. Ser. 254, 111–128.
McSweeney, J.M., Chant, R.J., Wilkin, J.L., Sommerfield, C.K., 2016. Suspended-sediment impacts on light-limited productivity in the Delaware Estuary. Estuar. Coast.
Munk, W.H., Anderson, E.R., 1948. Notes on a theory of the thermocline. J. Mar. Res. 7, 276–295.
Murray, A.B., 2003. Contrasting the goals, strategies, and predictions associated with simplified numerical models and detailed simulations. In: Wilcock, P.R., Iverson, R.M. (Eds.), Prediction in Geomorphology. American Geophysical Union, Washington, D. C.. https://doi.org/10.1029/135GM11
Murray, A.B., Thieler, E.R., 2004. A new hypothesis and exploratory model for the formation of large-scale inner-shelf sediment sorting and "rippled scour depressions". Continent. Shelf Res. 24, 295–315.
Muylaert, K., Sabbe, K., 1999. Spring phytoplankton assemblages in and around the maximum turbidity zone of the estuaries of the Elbe (Germany), the Schelde (Belgium/The Netherlands) and the Gironde (France). J. Mar. Syst. 22, 133–149.
Naithani, J., de Brye, B., Buyze, E., Vyverman, W., Legat, V., Deleersnijder, E., 2016. An ecological model for the Scheldt estuary and tidal rivers ecosystem: spatial and temporal variability of plankton. Hydrobiologia 775, 51–67.
Pennock, J.R., Sharp, J.H., 1994. Temporal alternation between light- and nutrient-limitation of phytoplankton production in a coastal plain estuary. Mar. Ecol. Prog. Ser. 111, 275–288.
Press, W.H., Flannery, B.P., Teukolsky, S.A., Vetterling, W.T., 1992. Numerical Recipes. Cambridge University Press.
Riley, G.A., 1967. The plankton of estuaries. In: Lauff, G. (Ed.), Estuaries. Elsevier, Washington DC, pp. 316–326.
Sarthou, G., Timmermans, K.R., Blain, S., Treguer, P., 2005. Growth physiology and fate of diatoms in the ocean: a review. J. Sea Res. 53, 25–42.
Sverdrup, H.U., 1953. On conditions for the vernal blooming of phytoplankton. J Conseil Exp Mer 18, 287–295.
Talke, S.A., de Swart, H.E., de Jonge, V.N., 2009a. An idealized model and systematic process study of oxygen depletion in highly turbid estuaries. Estuar. Coast 32, 602–620.
Talke, S.A., de Swart, H.E., Schuttelaars, H.M., 2009b. Feedback between residual circulations and sediment distribution in highly turbid estuaries: an analytical model. Physics of Estuaries and Coastal Seas 29, 119–135.
Tilman, D., Kilham, S.S., Kilham, P., 1982. Phytoplankton community ecology: the role of limiting nutrients. Annu. Rev. Ecol. Systemat. 13, 349–372.
Warner, J.C., Geyer, W.R., Lerczak, J.A., 2005. Numerical modeling of an estuary: a comprehensive skill assessment. J. Geophys. Res. 110 https://doi.org/10.1029/2004JC002,691. C05,001.